Journal of Sound and Vibration (1992) **154**(3), 411–429

VIBROACOUSTICAL ENERGY FLOW THROUGH STRAIGHT PIPES

G. PAVIĆ†

Centre Technique des Industries Mécaniques, F-60304 Senlis, France

(*Received* 28 *August* 1990, *and in revised form* 4 *March* 1991)

At lower relative (i.e., non-dimensional) frequencies, four propagating waves exist in fluid-filled pipes. Each of these waves carries energy in the pipe wall, while three waves carry energy in the fluid as well. The otherwise fairly complex dispersion laws for waves in pipes simplify in the frequency region considered to simple rod- and beam-type laws. It is shown that these laws can be determined by approximate formulae fairly accurately, the accuracy decreasing with increase in frequency. Due to fluid–wall coupling, expressed again by simplifications, the energy flow in both the wall and the fluid can be evaluated in principle from knowledge of surface vibrations only. The portions of the flow in the solid and the fluid fluctuate along the pipe axis, and consequently spatial averaging has to be done in order to obtain useful results. In this way, the pipe becomes a homogeneous one-dimensional waveguide, suitable for measurements of energy flow by detection of surface vibrations only. Specific transducer patterns for this purpose are described. At higher frequencies however, where additional propagating waves take place, simplifications are no longer possible. The exact expression for the unit-length energy flow can be then employed in conjunction with averaging around the circumference to evaluate flow in the wall at a particular axial position.

1. INTRODUCTION

Structural vibrations of a straight pipe exhibit a two-dimensional modal pattern, consisting of circumferential modes of orders $n=0, 1, 2, \ldots$ and the associated axial modes. For a pipe filled with a fluid, to each of the circumferential modes there corresponds an unlimited number of axial modes which can have either purely real, purely imaginary or complex wavenumbers. The extent to which individual modal pairs are excited depends on the frequency and the spatial distribution of the excitation.

At frequencies much below the ring frequency, $\Omega=\omega/\omega_r \ll 1$,‡ only the $n=0$ and $n=1$ modes (called pulsating and bending modes respectively) allow formation of purely real axial modes: i.e., wave propagation without spatial attenuation. This fact is relevant for energy flow in the pipe in view of the importance of propagating waves for energy transfer. The ring frequency, $\omega_r=c_s/a$, is fairly high for pipes of common sizes and materials, thus the condition $\Omega \ll 1$ will usually hold for the low- to mid-frequency range.

The pulsating mode, $n=0$, can propagate three distinct axial modes at $\Omega \ll 1$. One of these represents pure torsion, exhibiting only tangential motion uncoupled from two remaining orthogonal motions, axial and radial. The two other axial modes are free of tangential motion, but are coupled in the axial and radial directions. The bending mode, $n=1$, is characterized by lateral movements of the pipe, such that its cross-section remains virtually undeformed. In this mode, all three orthogonal motions are coupled.

† Formerly at the Electrotechnical Institute, Zagreb, Croatia.
‡ A list of symbols is given in Appendix III.

0022-460X/92/090411+19 $03.00/0

Corresponding to each modal pair of wall vibrations, there exists one modal pair which governs the motion of the contained fluid. Due to compatibility conditions, the axial wavelengths and the radial movements in the wall and in the fluid are equal at the interfacing surface, which in turn determines the pressure distribution inside the pipe. Therefore, a detailed enough knowledge of pipe wall vibrations enables an evaluation to be made of the energy flow along both the solid and the fluid parts.

It follows that the vibroacoustical energy flow along an existing pipe can be detected by an appropriate measurement and signal processing procedure. The main difficulty of formulating such a procedure results from the fact that there exists an interchange of energy along the pipe not only between different modes but between the solid and the fluid as well.

The modal behaviour of fluid-filled elastic cylindrical shells has been analyzed in references [1] and [2]. A very detailed account of vibroacoustical energy propagation along such shells, based on a modal approach, was given in references [3] and [4]. These works have revealed a fairly complex behaviour of the shell, even in the low frequency region. However, the majority of authors working on energy flow in pipes related to practical applications (see e.g., references [5–7]) prefer to use simplified pipe concepts (beam–rod or single-component impedance models). Energy flow in pipes was treated in more depth in reference [8], where theoretical considerations were supplemented by error analysis and experimental work. Both the pulsating and the bending modes were taken into account; however, the "acoustic" axial mode (one of the two non-torsional axial modes corresponding to $n=0$) has not been covered to the same extent as the other modes. The experimental procedures require matched accelerometers of very low cross-sensitivity.

In reference [9], formulae were presented in terms of physical rather than modal displacements, for intensity in a circular cylindrical shell. These were used in reference [10] for a low frequency formulation of energy flow through fluid-filled pipes vibrating in the $n=0$ mode. In both references [8] and [10] the importance of axial motions in energy propagation through pipes, which has often been neglected, was emphasized.

2. VIBROACOUSTICAL LOW FREQUENCY CHARACTERISTICS OF A FLUID-FILLED PIPE

The four characteristic axial propagating modes taking place in a fluid-filled pipe at low frequencies shall be denoted as follows: l, or longitudinal, mode, pertaining to $n=0$; a, or acoustical, mode, $n=0$; t, or torsional, mode, $n=0$; b, or bending, mode, $n=1$. The axial wavenumbers pertaining to these modes are the real solution of the dispersion equation. In this work, the equation based on Flügge's model is used (see Appendix I). At low frequencies, the wavenumbers can be represented by the following simple expressions, derived from the approximate dispersion equations for $n=0$ and $n=1$ given in Appendix I:

$$\kappa_l \simeq \zeta_l \Omega, \qquad \kappa_a \simeq \zeta_a \Omega, \qquad \kappa_t = \zeta_t \Omega, \qquad \kappa_b \simeq \zeta_b \sqrt{\Omega}. \tag{1}$$

Here $\kappa = k_x a$ is a non-dimensional representation of the axial wavenumber k_x, while the subscripts l, a, t and b refer to the four types of modes as specified above. The constants ζ are

$$\zeta_l = (1+\Delta)^{1/2}, \qquad \zeta_a = [\psi + (2\eta + \nu^2)/(1-\nu^2)]^{1/2},$$

$$\zeta_t = [2/(1-\nu)]^{1/2}, \qquad \zeta_b = (2+\eta)^{1/4},$$

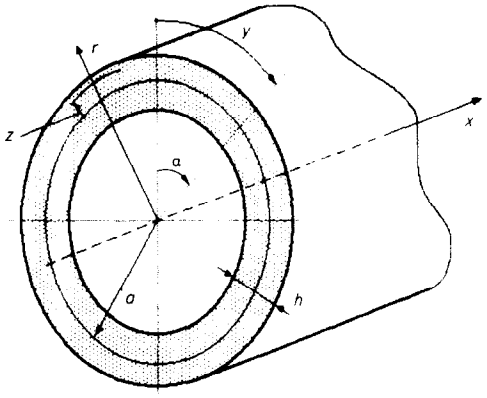

Figure 1. Co-ordinate system for the shell.

with (see Figure 1)

$$\psi=(c_s/c_f)^2, \qquad \eta=(\rho_f/\rho_s)(a/h), \qquad \Delta=\nu^2(\psi-1)/[(\psi-1)(1-\nu^2)+2\eta+\nu^2].$$

In accordance with the nature of the equations of motion for the circular cylindrical shell [11], the three orthogonal components of the wall motion at the middle surface, axial (u), tangential (v) and radial (w), can be expressed in terms of the four wave components as

$$\begin{aligned}\mathbf{u}&=\mathrm{j}U_{l+}\boldsymbol{\mu}_{l+}+\mathrm{j}U_{l-}\boldsymbol{\mu}_{l-}+\mathrm{j}U_{a+}\boldsymbol{\mu}_{a+}+\mathrm{j}U_{a-}\boldsymbol{\mu}_{a-}+\mathrm{j}U_{b+}\boldsymbol{\mu}_{b+}\cos\vartheta_{+}+\mathrm{j}U_{b-}\boldsymbol{\mu}_{b-}\cos\vartheta_{-},\\ \mathbf{v}&=V_{t+}\boldsymbol{\mu}_{t+}+V_{t-}\boldsymbol{\mu}_{t-}+V_{b+}\boldsymbol{\mu}_{b+}\sin\vartheta_{+}+V_{b-}\boldsymbol{\mu}_{b-}\sin\vartheta_{-},\\ \mathbf{w}&=W_{l+}\boldsymbol{\mu}_{l+}+W_{l-}\boldsymbol{\mu}_{l-}+W_{a+}\boldsymbol{\mu}_{a+}+W_{a-}\boldsymbol{\mu}_{a-}+W_{b+}\boldsymbol{\mu}_{b+}\cos\vartheta_{+}+W_{b-}\boldsymbol{\mu}_{b-}\cos\vartheta_{-}.\end{aligned} \tag{2}$$

where $\boldsymbol{\mu}$ denotes the propagation factor, and ϑ defines the polarization of the bending waves:

$$\boldsymbol{\mu}_{q\pm}=\exp(\mp\mathrm{j}\kappa_q x/a+\mathrm{j}\varphi_{q\pm}), \qquad q=l,a,t,b, \quad \vartheta_{\pm}=\alpha-\gamma_{\pm}.$$

The wave amplitudes U, V and W are real quantities, while the components $\mathbf{u}$, $\mathbf{v}$ and $\mathbf{w}$ are complex (indicated by bold symbols). The three equations for the displacements, (2), are given in a form which allows the most general conditions of wave motion under the assumptions specified before, and yet satisfies the equations of wall motion [11] for the dynamic conditions. In particular, wave propagation is assumed in both directions, while for oppositely moving bending wave components different polarization angles are allowed.

Waves in the fluid contained within the pipe are of the same type as the waves in the solid, with the exception of the torsional waves which cannot exist in the fluid. The acoustical pressure in the fluid, represented by a characteristic radial distribution [12], assumes in this case the following form, obtained by a small-argument expansion of Bessel functions:

$$\begin{aligned}\mathbf{p}&=[1-\xi_l^2(r/a)^2/4](P_{l+}\boldsymbol{\mu}_{l+}+P_{l-}\boldsymbol{\mu}_{l-})+[1-\xi_a^2(r/a)^2/4](P_{a+}\boldsymbol{\mu}_{a+}+P_{a-}\boldsymbol{\mu}_{a-})\\ &\quad+(\xi_b/2)(r/a)(P_{b+}\boldsymbol{\mu}_{b+}\cos\vartheta_{+}+P_{b-}\boldsymbol{\mu}_{b-}\cos\vartheta_{-}).\end{aligned} \tag{3}$$

Here P are the acoustical pressure amplitude maxima (located along the axis for l and a waves and at the wall for b waves), while ξ is the normalized radial wavenumber which, satisfying the formula $\xi^2=\psi\Omega^2-\kappa^2$, can assume either imaginary or real values for real κ. By virtue of the equation of fluid motion and of the compatibility conditions at the fluid–solid interface, relationships can be established between the motions in the fluid and in the pipe wall.

3. RELATIONSHIPS BETWEEN WAVE AMPLITUDES

The displacement amplitudes U, V, W and the pressure amplitudes P stand in a firm relationship for any modal pair, which results from the equations of pipe motion [11]. For low values of frequency Ω, the displacement relationships simplify to (see Appendix I)

$$U_{l\pm} = \mp \Gamma_l / \Omega W_{l\pm}, \qquad U_{a\pm} = \mp \Gamma_a / \Omega W_{a\pm}, \qquad U_{b\pm} = \pm \zeta_b \sqrt{\Omega}\, W_{b\pm}, \qquad V_{b\pm} = -W_{b\pm}, \quad (4)$$

where $\Gamma = \nu\zeta/(\zeta^2 - 1)$.

It can be seen from equations (4) that the amplitudes of axial wave components of the longitudinal mode, $U_{l\pm}$, have to be much larger than the amplitudes of the corresponding radial components $W_{l\pm}$, since $\Omega \ll 1$ and $\Gamma_l \approx 1/\nu$ or smaller. The opposite applies to the bending mode where radial (and thus tangential) motions dominate. This implies that measurements of longitudinal and bending modes have to be done by detecting the axial and the radial motions respectively.

Concerning the acoustical mode, a unique conclusion regarding the ratio of the axial and radial component amplitudes cannot be drawn. The limiting frequency $\Omega_{u=w} = \Gamma_a$ exists according to equations (4) below which the axial motions are larger and above which the opposite applies. If the pipe behaviour approaches that of a rigid duct, where $\zeta_a \approx \sqrt{\psi} = c_s/c_f$ (upon assuming $c_s \gg c_f$), the limiting frequency will be mainly unaffected by the pipe geometry since in this case $\Gamma_a \approx (\nu c_f)/(c_s)$. This condition applies to light fluids, i.e., gases, unless the pipe is extremely thin. In other cases, the limiting frequency gradually rises with the pipe thickness, as shown in Figure 2 for the cases of pipes made of steel or hard rubber and filled with water (for the sake of comparison, the curves for pipes containing air compressed to 10 bar instead of water are also shown).

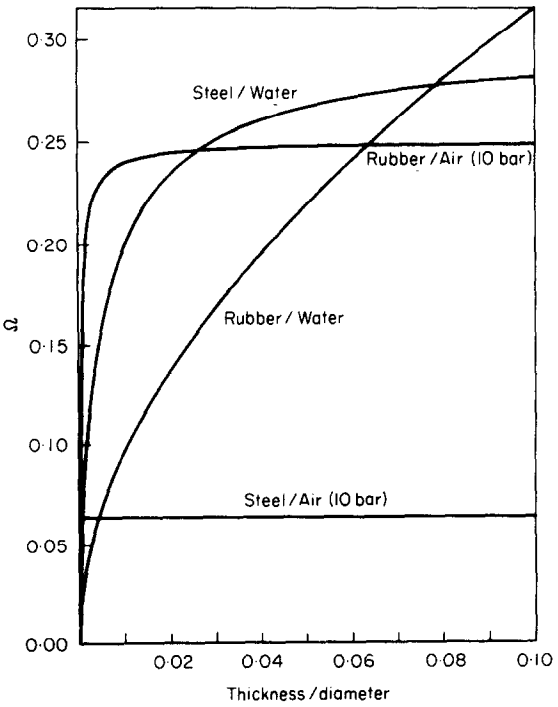

Figure 2. Frequency of equal axial and radial amplitudes of a types of waves.

The acoustical pressure amplitudes become related to the radial displacement amplitudes via the following expressions derived from reference [3] on basis of low frequency and small wavenumber values:

$$P_{l\pm} = -2\rho_f c_s^2 \Omega^2 / (\xi_l^2 a) W_{s\pm}, \qquad P_{a\pm} = -2\rho_f c_s^2 \Omega^2 / (\xi_a^2 a) W_{f\pm},$$

$$P_{b\pm} = 2\rho_f c_s^2 \Omega^2 / (\xi_b a) W_{b+} \tag{5}$$

4. VALIDITY OF LOW FREQUENCY ASSUMPTIONS

The low frequency assumptions, made so far, limit the validity of the analysis to the region where (a) simplified dispersion expressions for various wave types, (1), are tolerable and (b) the $n=2$ mode cut-on frequency lies above the upper frequency limit.

The first condition, (a), will be dictated by the quality of approximation (1) referring to the bending-wave axial wavenumber, κ_b, as this approximation is less accurate than the approximations for the pulsating mode wavenumbers. In Figure 3 is shown the bending wavenumber error, given as the ratio of the approximate and the exact κ_b values in dB units, for infinitely thin pipes vibrating *in vacuo*, where the error depends only on the frequency and the Poisson ratio. The exact solution of the dispersion equation (see Appendix I) was evaluated for this and the forthcoming examples using a numerical programme.

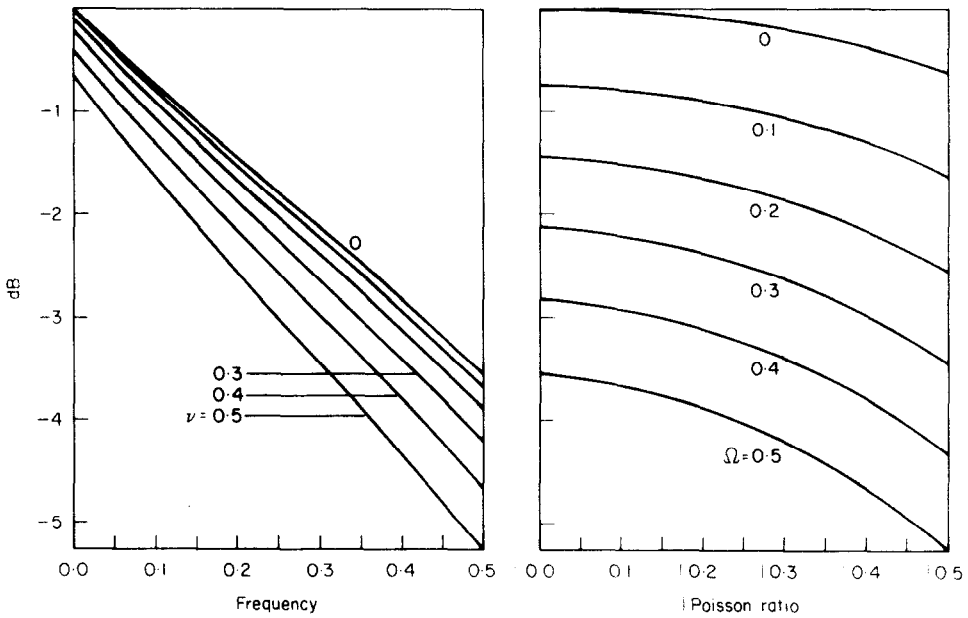

Figure 3. Error in bending wavenumber formula (1): infinitely thin pipe vibrating *in vacuo*.

The example shown is representative of all situations where the fluid loading is relatively small (in which case the thickness becomes largely unimportant for the wavenumber). It can be seen that the error increases with frequency (as expected) but also with ν (which was not so obvious). Even with frequency reducing to zero the error exists, but for the trivial case $\nu=0$. For $\nu=0{\cdot}3$, which is representative of most metals, the 10% difference in the approximate and exact solutions ($\approx$1 dB), taken here as the tolerance limit, occurs at frequency $\Omega \approx 0{\cdot}09$.

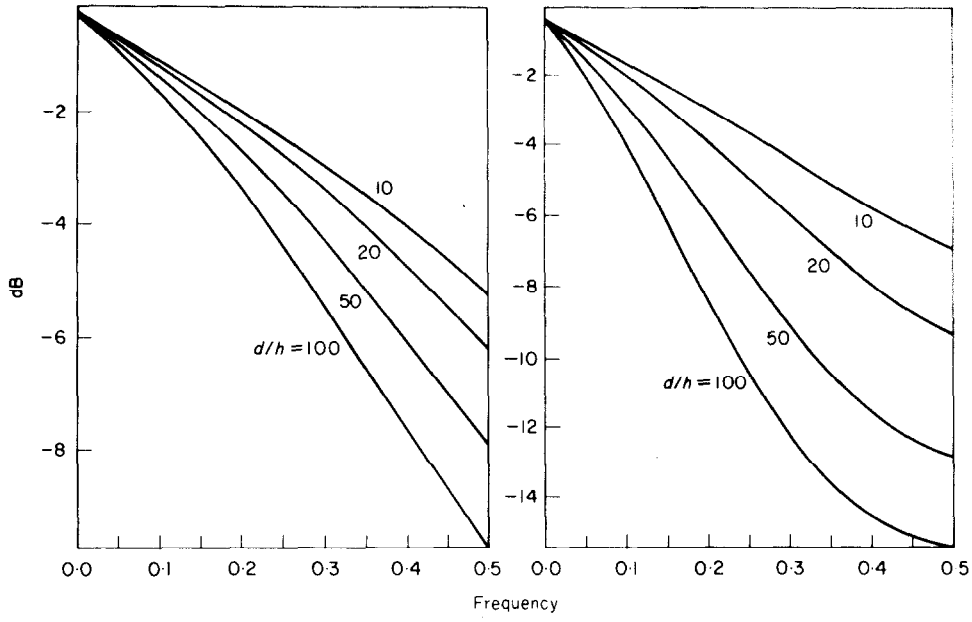

Figure 4. Error in bending wavenumber formula for water-filled pipes: left, steel pipe; right, hard rubber pipe.

The same error is shown for the case of a water-filled pipe in Figure 4. Case (a)—a steel pipe—is an example of moderate fluid loading, while case (b)—a hard rubber pipe—represents high loading. As expected, the error increases with decreasing thickness. The more the thickness decreases, the more the mechanical properties of the pipe depart from the Euler–Bernoulli bending model which the corresponding formula in equation (1) actually represents. Given the range of thicknesses between 1/10 to 1/100 of the diameter, the 1 dB error lies between $\approx 0{\cdot}09$ and $\approx 0{\cdot}06$ for steel and between $\approx 0{\cdot}05$ and $\approx 0{\cdot}02$ for rubber pipes. This shows that the approximate formula for the bending wavenumber, based on the Euler–Bernoulli model, is of modest accuracy, despite the fact that fluid loading of the pipe is represented in this formula in a way that is consistent with the model: i.e., as an added mass.

The accuracy of wavenumber approximations for $n = 0$ modes is much higher. The case, analogous to the one from Figure 3 (zero thickness, zero fluid loading), which refers to *l* waves, is exactly represented by $\kappa_l = \Omega\sqrt{1 + \nu^2/(1 - \nu^2 - \Omega^2)}$, and approximation becomes thus unnecessary. In Figures 5–7 are shown the errors of the wavenumber approximation for both *l* and *a* type waves, for some characteristic pipe–fluid combinations. Unlike the errors for other types of waves, the error for *l* waves in these examples is shown as the ratio between the approximate and the accurate values of $\sqrt{\kappa_l^2 - \Omega^2}$, instead of simply κ_l values. The reason for such a representation is in the fact that the relative wavenumber of *l* waves, κ_l, is usually close to Ω, implying that the dispersion constant, ζ_l (see equation (1)) is close to 1. Since some important relationships concerning energy flow are given in terms of the quantity $\Gamma_l \propto 1/(\zeta_l^2 - 1) \propto 1/(\kappa_l^2 - \Omega^2)$, it is this difference which matters more than the wavenumber itself.

The approximation error related to water-filled steel pipes (Figure 5) depends much more on thickness for *a* waves than for *l* waves. The latter error is almost independent of thickness in the relevant 0–1 dB region. The *a* wave error, on the contrary, depends very much on thickness. The approximations used are seen to be consistent:† the error vanishes

† An approximate formula relating the phase velocity of *a* waves to frequency [13] is more accurate than the simple formula (1) at higher frequencies, but it lacks consistency at low frequencies as it does not converge to the exact solution with frequency reducing to zero.

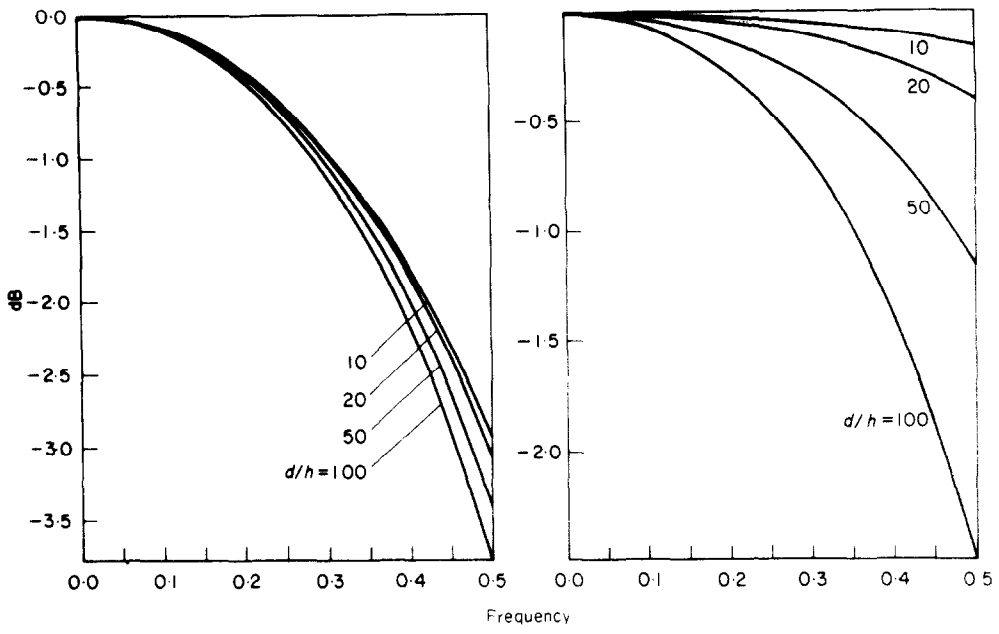

Figure 5. Error in wavenumber formula for pulsating mode of water-filled steel pipes: left, *l* waves; right, *a* waves.

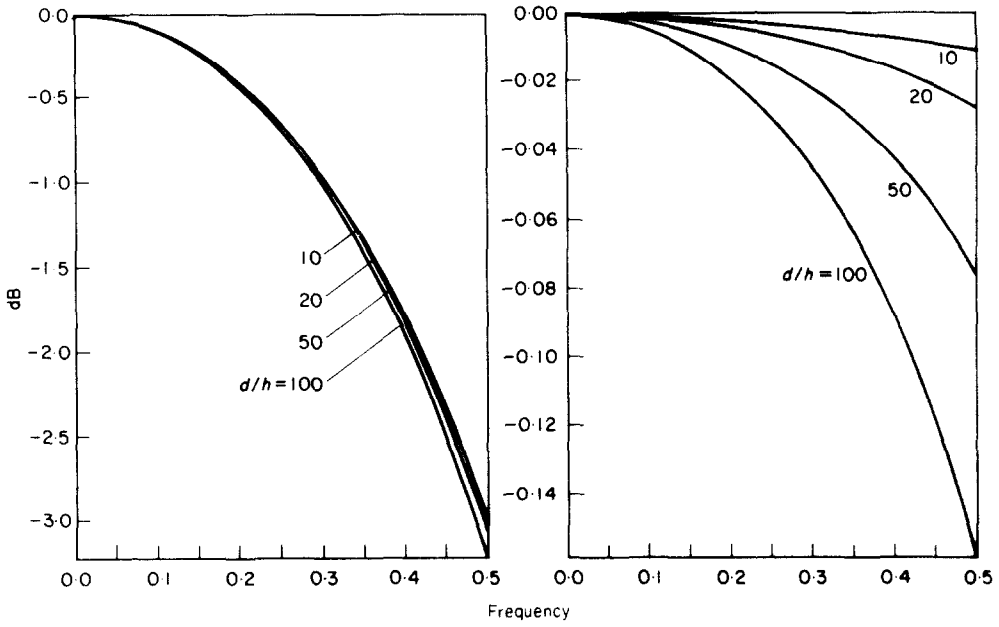

Figure 6. Error in wavenumber formula for pulsating mode of rubber pipes containing compressed air (10 bar): left, *l* waves; right, *a* waves.

as the frequency approaches zero for both types of waves. The "usable" frequency range is here quite broad, 0·3 for *l* waves and from 0·3 to above 0·5 (depending on thickness) for *a* waves.

Very similar results apply to rubber pipes containing compressed air (Figure 6). The range of thickness displayed (1/100 to 1/10 of the diameter) was chosen to show the influence of various parameters, although thin rubber pipes subjected to internal pressure

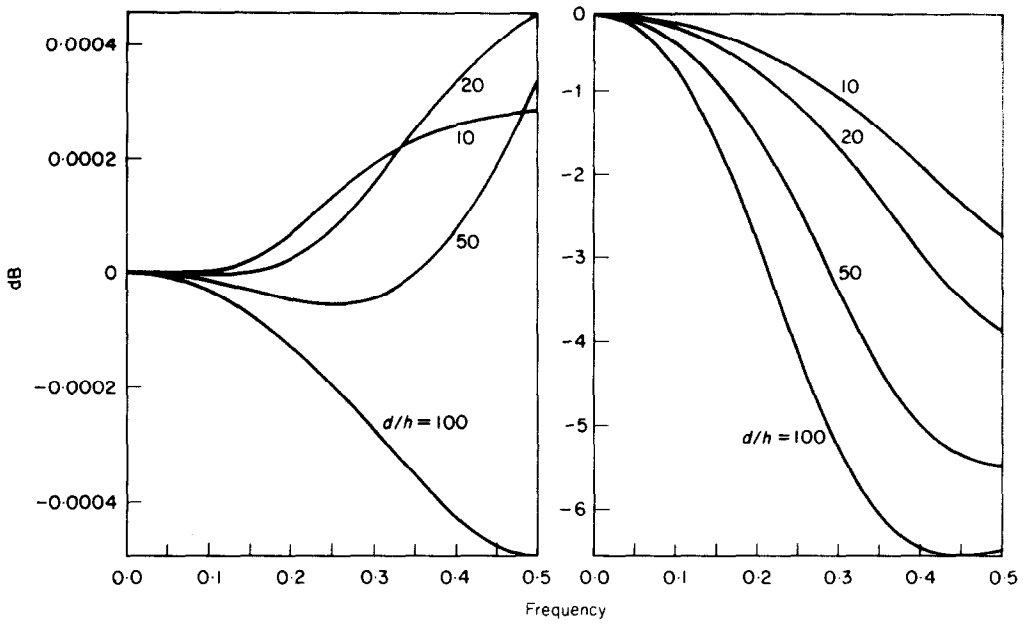

Figure 7. Error in wavenumber formula for pulsating mode, *a* waves: left, steel pipe containing compressed air (10 bar); right, rubber pipe filled with water.

are of no practical interest. In the cases where mismatch between properties of the pipe material and the fluid (mass density and sound velocity) is either extremely large (Figure 7(a)—steel/compressed air), or very small (Figure 7(b)—rubber/water), the approximations for the wavenumber of *a* waves are either extremely good (a) or modest (b).

It can be concluded that the approximate formulae (1) are generally applicable to lower frequencies and thicker pipes. When using these formulae, care should be taken with the degree of matching of properties between the pipe material and the fluid and, where necessary, a more accurate solution of the dispersion equation than the one given by equation (1) should be employed.

Above the cut-on frequency of the $n=2$ mode, the previous results remain the same, but an additional wave type appears, which makes an analysis of pipe motion much more complex for a number of reasons. The cut-on frequency is reported as being clearly noticeable in measurements [8]. It therefore becomes important to determine this frequency with sufficient accuracy.

The cut-on frequency for any particular mode n can be evaluated from the dispersion equation (A1) by setting κ to zero:

$$(n^2-\Omega^2)[1-\Omega^2-Fl+\beta^2(n^2-1)^2]-n^2=0. \tag{6}$$

For $n>0$ and Ω, $\kappa \ll 1$, the fluid loading becomes proportional to frequency square, $Fl=\eta\Omega^2/n$ (see Appendix I). The solution of equation (6) then can be approximated by a linear equation in Ω^2:

$$\Omega^2_{cut\text{-}on}=\beta^2n^2(n^2-1)^2/[1+n^2(1+\eta/n)+\beta^2(n^2-1)^2]. \tag{7}$$

This solution holds for small to medium values of η (i.e., for not too thin pipes). In such a case, the cut-on frequency exhibits an almost linear dependence on thickness. By neglecting the term in square brackets containing β^2, and setting $n=2$, a simple formula is obtained, as already reported [14].

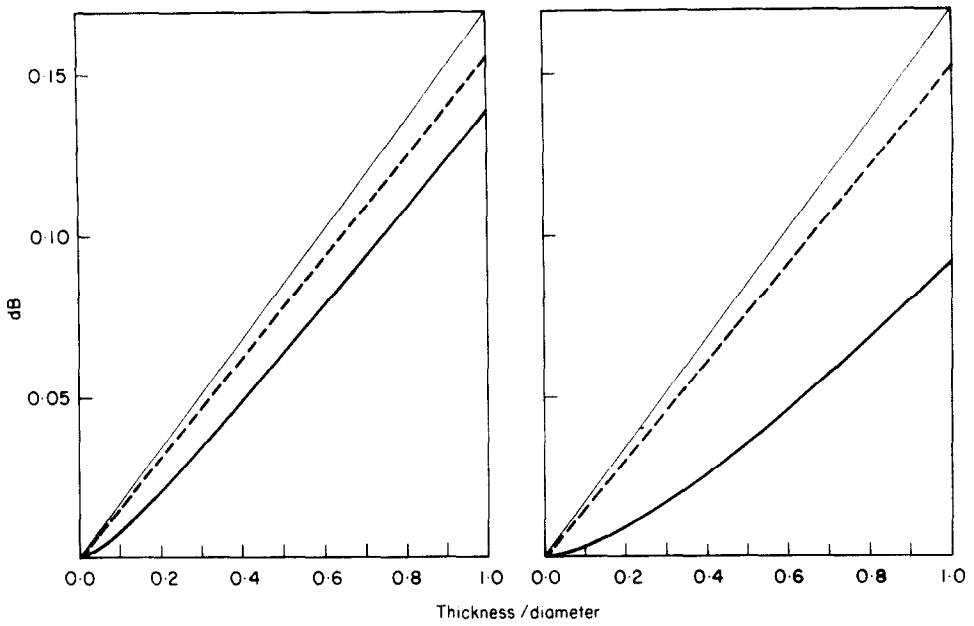

Figure 8. Cut-on frequency of $n=2$ mode: left, steel pipe; right, hard rubber pipe. Full thin line, vacuum; dotted line, compressed air (10 bar); full thick line, water.

In Figure 8 is shown the dependence of the lowest cut-on frequency, i.e., the one for $n=2$, on the thickness to diameter ratio for (a) steel and (b) rubber pipes containing vacuum, 10 bar pressurized air and water. The frequency increases with thickness, but decreases with mass density of the contained fluid. The diagrams represent the exact solution for the cut-on frequency; the approximate values obtained from equation (7) differ by no more than 0·24% for the cases considered.

5. ENERGY FLOW

Given in terms of middle surface displacement components, the energy flow in axial direction per unit circumferential length in the wall of a circular cylindrical shell reads [15]

$$H_s^1 = H^0(\bar{\Lambda}_e + \bar{\Lambda}_f + \bar{\Lambda}_c), \qquad H^0 = E_s h/(1-\nu^2). \tag{8}$$

The energy flow factors, extensional Λ_e, flexural Λ_f and curvature-dependent Λ_c read

$$\Lambda_e = -\overline{(\partial u_0/\partial x + \nu\,\partial v_0/\partial y)\dot{u}_0} - \{(1-\nu)/2\}\overline{(\partial u_0/\partial y + \partial v_0/\partial x)\dot{v}_0},$$

$$\Lambda_f = (h^2/12)[\overline{\{\partial(\Delta w_0)/\partial x\}\dot{w}_0} - \overline{(\partial^2 w_0/\partial x^2 + \nu\,\partial^2 w_0/\partial y^2)\,\partial\dot{w}_0/\partial x}$$
$$- (1-\nu)\overline{(\partial^2 w_0/\partial x\,\partial y)\,\partial\dot{w}_0/\partial y}],$$

$$\Lambda_c = -(1/a)[\nu\overline{w_0\dot{u}_0} + (h^2/12)\{\nu\overline{(\partial^2 w_0/\partial y^2)\dot{u}_0}$$
$$- [(1-\nu)/2]\overline{[(1/a)(\partial u_0/\partial y - \partial v_0/\partial x) + \partial^2 w_0/\partial x\,\partial y]\dot{v}_0}$$
$$- [(1-\nu)/2]\overline{\{\partial(\partial u_0/\partial y - \partial v_0/\partial x)/\partial y\}\dot{w}_0} - (\nu/a)\overline{(\partial w_0/\partial x)\dot{w}_0} + (\nu/a)\overline{w_0\,\partial\dot{w}_0/\partial x}$$
$$+ [(1-\nu)/2]\overline{(\partial u_0/\partial y - \partial v_0/\partial x)\,\partial\dot{w}_0/\partial y}\}]. \tag{9}$$

The total flow in the wall is obtained by averaging the unit flow H_s^1 around the circumference, denoted here by $\langle\ \rangle_y$:

$$H_s(x)=\int_0^{2\pi a} H_{s,x}^1(x,y)\,\mathrm{d}y=2\pi a H^0(\langle\Lambda_e\rangle_y+\langle\Lambda_f\rangle_y+\langle\Lambda_c\rangle_y). \tag{10}$$

After applying expressions (8) and (10) to the low frequency pipe motion, expressed in terms of modal superposition (equations (2)), formulae are obtained for the energy flow factors which contain the x co-ordinate as a variable. While the total energy flow through the pipe does not depend on x throughout any sourceless, lossless region represented by equations (2), there exists an interchange of a portion of the total energy between the pipe wall and the fluid, as already reported [9]. It is therefore convenient to operate with axially averaged energy flow values. After the axial averaging is done, the three factors assume the following form:†

$$\begin{aligned}
\langle\Lambda_e\rangle_{y,x}&=(\omega/2a)\{\kappa_l(U_{l+}^2-U_{l-}^2)+\kappa_a(U_{a+}^2-U_{a-}^2)\\
&\quad+((1-\nu)/2)\kappa_t(V_{t+}^2-V_{t-}^2)+(\kappa_b/2)[(U_{b+}^2-U_{b-}^2)+((1-\nu)/2)(V_{b+}^2-V_{b-}^2)]\\
&\quad+((1+\nu)/4)(U_{b+}V_{b+}+U_{b-}V_{b-})\},\\
\langle\Lambda_f\rangle_{y,x}&=(\omega/a)\beta^2[\kappa_l^3(W_{l+}^2-W_{l-}^2)+\kappa_a^3(W_{a+}^2-W_{a-}^2)+\kappa_b((1+\kappa_b^2)/2)(W_{b+}^2-W_{b-}^2)],\\
\langle\Lambda_c\rangle_{y,x}&=(\omega/2a)[\nu\{(1+\beta^2)[(U_{l+}W_{l+}+U_{l-}W_{l-})+(U_{a+}W_{a+}+U_{a-}W_{a-})]\\
&\quad+\tfrac{1}{2}[1-\beta^2((1-\nu)/\nu)](U_{b+}W_{b+}+U_{b-}W_{b-})\}+\beta^2\{\cdots\}].
\end{aligned} \tag{11}$$

Since $\beta^2\ll 1$, the terms containing β^2 can be neglected in comparison to unity, which is always the case for low frequency motion. By expressing each particular wave type through only one of the orthogonal components of motion, using the established coupling relationships (4), and by additionally neglecting the low order terms, the expression for energy flow in the wall assumes the following simple form:

$$\begin{aligned}
H_s&=\pi E_s/(1-\nu^2)(h/a)c_s\Omega^2[\zeta_l(U_{l+}^2-U_{l-}^2)+\zeta_a(U_{a+}^2-U_{a-}^2)\\
&\quad+((1-\nu)/2)\zeta_t(V_{t+}^2-V_{t-}^2)+\zeta_b^3\sqrt{\Omega}(W_{b+}-W_{b-})].
\end{aligned} \tag{12}$$

Energy flow in the fluid contained within the pipe can be obtained by directly integrating the axial component of sound intensity over the cross-section. Since the axial velocity of the propagating waves is proportional to the acoustic pressure,

$$\mathrm{j}\omega U_{q\pm}=\mathrm{j}/(\omega\rho_f)\,\partial p/\partial x=\pm\kappa_q/(\rho_f c_s\Omega)P_{q\pm},\qquad q=l,a,b,$$

the intensity, and thus the fluid energy flow, becomes proportional to the difference of the pressure amplitudes squared:

$$\begin{aligned}
\langle I(r)\rangle_{y,x}&=(1/2)\ \mathrm{Re}\ \{\mathbf{p}(r)\dot{\mathbf{u}}(r)^*\}\\
&=[1/(2\rho_f c_s\Omega)]\{\kappa_l[1-\xi_l^2(r/a)^2/4]^2(P_{l+}^2-P_{l-}^2)\\
&\quad+\kappa_a[1-\xi_a^2(r/a)^2/4]^2(P_{a+}^2-P_{a-}^2)+\kappa_b[\xi_b(r/2a)^2/2](P_{b+}^2-P_{b-}^2)\}.
\end{aligned} \tag{13}$$

† Because of fixed relationships between the three orthogonal displacement components, each of the four wave modes will be dealt with by using one of the components while expressing the others through the selected one. The "representative" component will be the one exhibiting the largest amplitude. For *a* type waves, the largest amplitude component will depend on the circumstances, as described. Here the axial component will be chosen as the representative one for *a* waves but, where appropriate, it can easily be converted to the radial one by using equation (4).

Upon integrating the axial component of intensity over the interior cross-section of the pipe, and subsequently expressing the acoustical pressure amplitudes in terms of the selected displacement component amplitudes via expressions (5) and (4), the fluid energy flow, averaged in the axial direction, becomes, after some simplifications,

$$H_f = [2\pi E_s/(1-\nu^2)](\rho_f/\rho_s)c_s\Omega^2[\{\zeta_l/(\psi-\zeta_l^2)^2/\Gamma_l^2\}(U_{l+}^2 - U_{l-}^2) + \{\zeta_a/(\psi-\zeta_a^2)^2/\Gamma_a^2\}(U_{a+}^2 - U_{a-}^2) + \zeta_b\{\Omega\sqrt{\Omega}/16\}(W_{b+}^2 - W_{b-}^2)]. \quad (14)$$

The averaged energy flow in the pipe wall and the fluid, given by equations (12) and (14), is seen to be a linear superposition of four characteristic differences of amplitude squares. The coefficients in the two energy expressions are simple functions of the pipe geometry and the solid and fluid material parameters. It follows that measurement of energy flow in a pipe reduces virtually to measurement of four differences of squared amplitudes.

6. MEASUREMENT OF ENERGY FLOW

The four differences of squared amplitudes which have to be detected in order to evaluate the total energy flow in the pipe, according to equations (12) and (14), are

$$L = U_{l+}^2 - U_{l-}^2, \qquad A = U_{a+}^2 - U_{a-}^2, \qquad T = V_{t+}^2 - V_{t-}^2, \qquad B = W_{b+}^2 - W_{b-}^2. \quad (15)$$

A straightforward way to determine the unknown quantities from equations (15) would consist of sampling the vibration field at a sufficient number of locations, and evaluating the unknowns from a set of the corresponding displacement equations (2). The problem is that equations (2) contain far more unknowns than needed for energy flow evaluation—eight wave amplitudes, eight wave phases and two polarization angles, i.e., 18 in total. This problem can be circumvented by use of an appropriate combination of measurement signals.

It should be noted that equations (2) refer to the mid-surface displacements, while any measurement has to be done at the outer pipe surface. Only the radial displacements are equal at the two surfaces, while the remaining two displacement components satisfy the following relationships [11]:

$$u = u_0 - (h/2)\,\partial w_0/\partial x, \qquad v = v_0 - (h/2)(\partial w_0/\partial y - v_0/a), \quad (16)$$

where the subscript zero denotes the mid-surface. If the superposition of displacements (either sum or difference), located at two diametrally opposite positions, α and $\alpha+\pi$, is introduced via

$$q^{\pm}(x,\alpha) = (1/2)[q(x,\alpha) \pm q(x,\alpha+\pi)], \qquad q = l, a, t, b, \quad (17)$$

the squared amplitudes differences T and B can be directly obtained by a suitable multiplication plus time-averaging procedure as follows:

$$T = 2a/[c_s\Omega \sin(2\zeta_t\Omega\delta/a)]\overline{\dot{v}^+(\delta,\alpha)v^+(-\delta,\alpha)},$$
$$B = 2a/[c_s\Omega \sin(2\zeta_b\sqrt{\Omega}\,\delta/a)][\overline{\dot{w}^-(\delta,\alpha)w^-(-\delta,\alpha)} + \overline{\dot{w}^-(\delta,\alpha+\pi/2)w^-(-\delta,\alpha+\pi/2)}]. \quad (18)$$

Here δ is an arbitrary spacing which determines the locations of measurement points about the reference position taken at $x=0$. The difference of squared torsional amplitudes is given by a single averaged product of the mean tangential velocity at $x=\delta$ and the mean tangential displacement at $x=-\delta$. The difference of squared bending amplitudes is given

by a sum of two similar products, composed of radial motions, to account for the polarization effect of bending waves. Here δ denotes the distance from $x=0$, which can be arbitrarily chosen as long as it stretches only within the zone where the wave equation assumption given by equations (2) holds.

Extraction of axial squared amplitudes is more complex than described so far for other wave types, because two axial wave types exist for the same circumferential mode $n=0$. Extraction can be done by measurement of mean axial motions u^+ at four axial locations (both in amplitude and phase), and determination of each individual axial amplitude by use of complex matrix algebra. It should be noted that mean displacements u^+, taken at the outer surface, are influenced not only by axial but also by radial displacements, as seen from equations (16). The relative influence of radial displacements can be found to be given by $(h/2a)(\zeta/\Gamma)\Omega^2$, which is so small a quantity that can be safely disregarded for $\Omega \ll 1$.

A particular extraction method, related to quantities L and A (i.e., axial squared amplitudes) is described in Appendix II. The method is based on detection of axial displacements and strains. Such a combination is appropriate for practical measurements in view of typical levels of the two quantities.

If the pipe is empty, only one of the two axial wave types exists (l type). In such a case the first of equations (18) applies for evaluation of the difference of squared amplitudes also for the axial mode, with v replaced by u and ζ_l replaced by ζ_l.

7. PARAMETERS OF ENERGY FLOW

The preceding analysis has shown that axial motions largely govern the energy flow in pipes at low relative frequencies. The major benefit of the modal approach in evaluation of energy flow, as described, is the possibility of detection of the fluid flow without any physical contact with the fluid. The fluid contribution to the energy flow due to the bending motion will usually be negligible in comparison with the solid contribution; the ratio between the two is a very small quantity, $\Omega\eta/[8\sqrt{2+\eta}]$, as can be evaluated from equations (12) and (14). The fluid contribution due to axial motion, however, can be very important. This contribution depends on the ratio of the amplitudes of l and a type of waves.

The effect of the variation of the amplitudes on the energy flow distribution in the pipe and the fluid can be considered by assuming for simplicity that propagation of the waves is in one direction only. It can be readily seen from equations (12) and (14) that the ratio of energy flow in the solid and the fluid cannot take any arbitrary value under the assumption of one-directional propagation. In Figure 9 is shown the range of the dependence of the solid-to-fluid energies ratio, presented in dB, in the thickness-to-diameter ratio for steel pipes filled with (a) water and (b) 10 bar compressed air. For water-filled pipes the range of this ratio is on average between +30 and −15 dB, while for air filled pipes it is much wider: +70 to −50 dB. The same quantity is shown in Figure 10 for hard rubber pipes, the ranges being much narrower due to a smaller mismatch between solid and fluid properties.

The possibility of practical detection of both solid and fluid energy flow from measurements on the external pipe surface depends on the ratio of amplitudes of l and a waves. If this ratio is higher than $\approx +30$ dB or lower than ≈ -30 dB one of the two waves will most probably remain undetected by usual measuring techniques. In Figures 11–14 is shown the dependence of the ratio of l and a amplitudes of the axial displacement on the ratio of solid–fluid energy flow and on the thickness-to-diameter ratio for pipe and fluid combinations from the preceding examples.

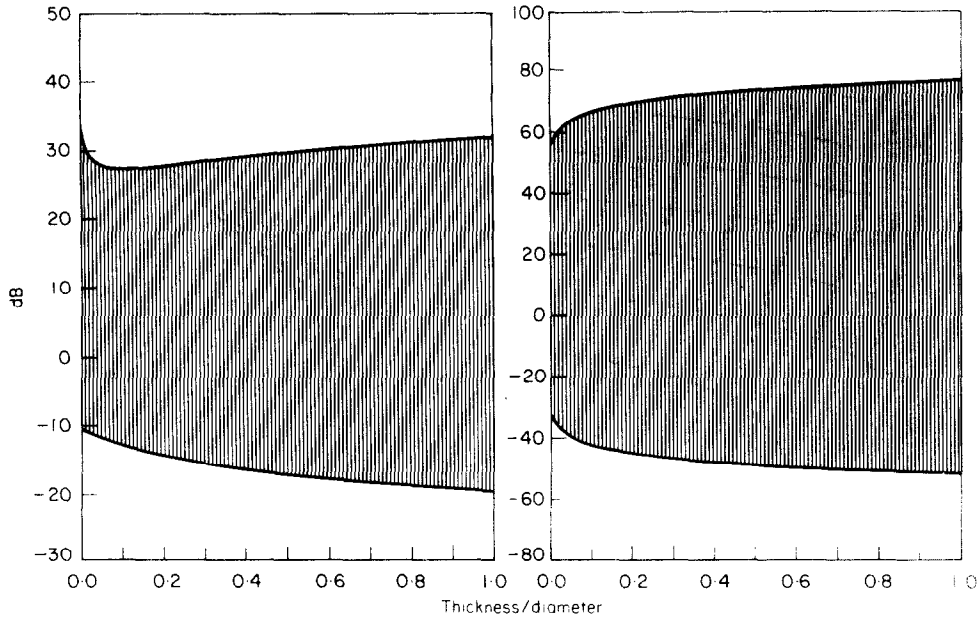

Figure 9. Ratio of energy flow in solid and fluid for steel pipes containing left, water, and right, compressed air (10 bar).

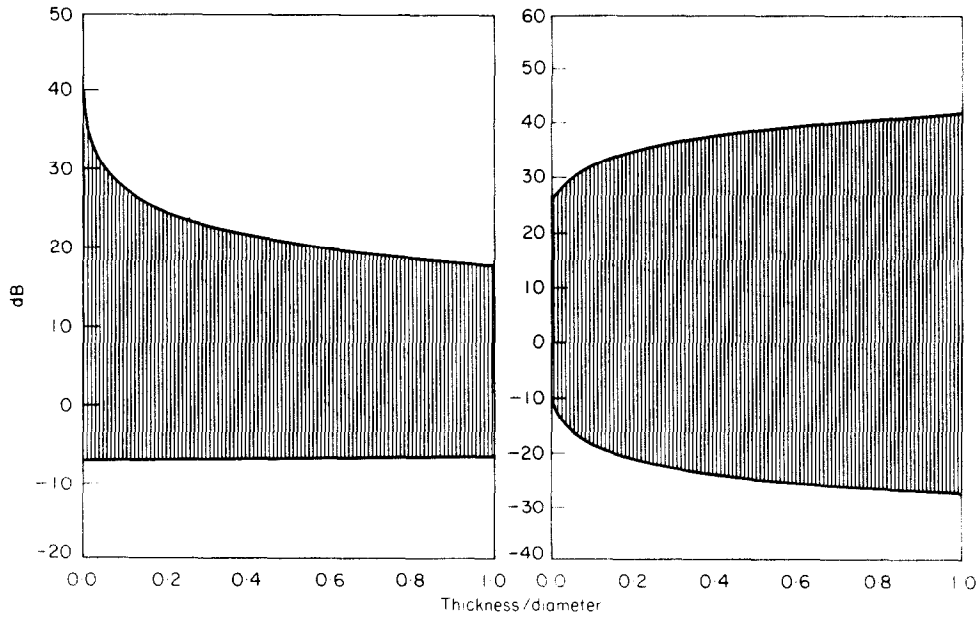

Figure 10. Ratio of energy flow in solid and fluid for rubber pipes containing left, water, and right, compressed air (10 bar).

According to the ±30 dB criterion of detectability of both axial waves in the pipe, the limiting ratio between energy flow in the solid and the fluid can be found to depend on the pipe thickness. For water-filled steel pipes the flow in the fluid can still be detected if it is 5–10 dB lower than in the pipe wall (Figure 11). The flow in the wall can always be detected, no matter how large the flow in the fluid. Pipes conveying 10 bar compressed air

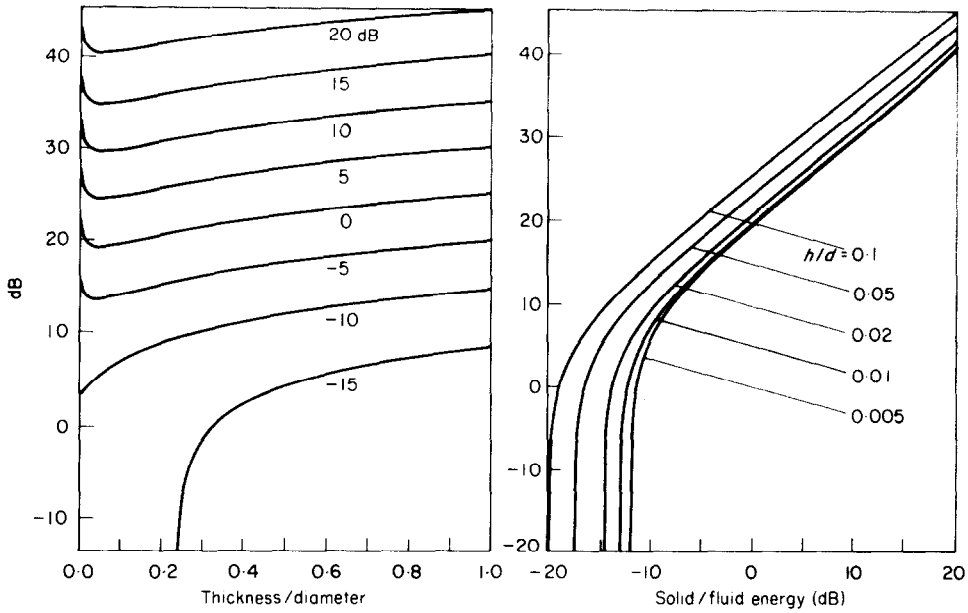

Figure 11. Ratio of amplitudes of *l* and *a* waves for steel pipes filled with water.

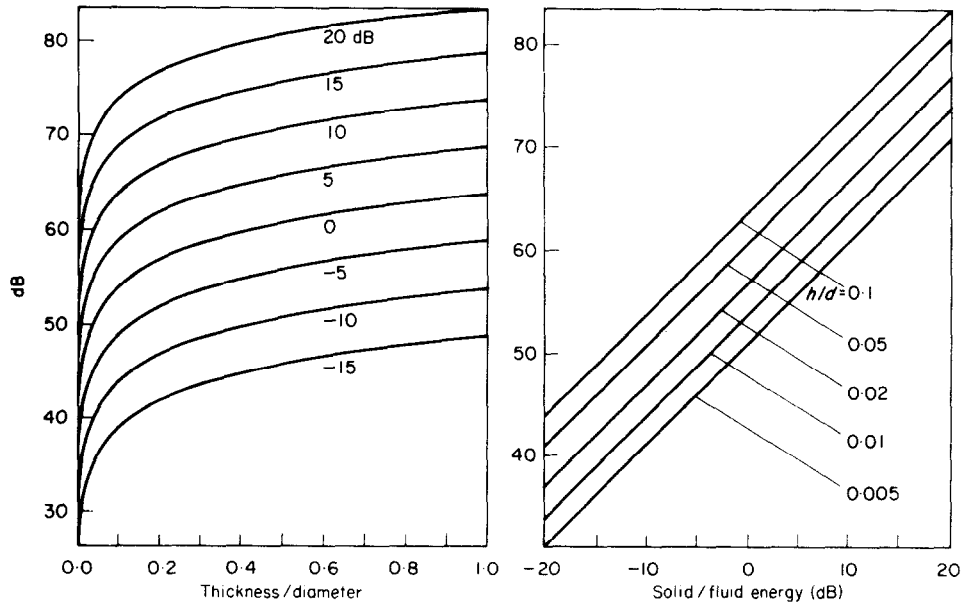

Figure 12. Ratio of amplitudes of *l* and *a* waves for steel pipes containing compressed air (10 bar).

can be successfully treated only if they are very thin, and if the flow in the fluid is more than 15–20 dB higher than in the wall (Figure 12). This results from very weak fluid–solid coupling. The good coupling which exists with rubber pipes filled with water makes detection of both axial waves possible provided that the flow in the solid is no more than 10–15 dB higher than in the water (Figure 13). Finally, the flow in compressed air contained in rubber pipes can be detected only if it exceeds the flow in the wall for realistic values of the thickness (Figure 14).

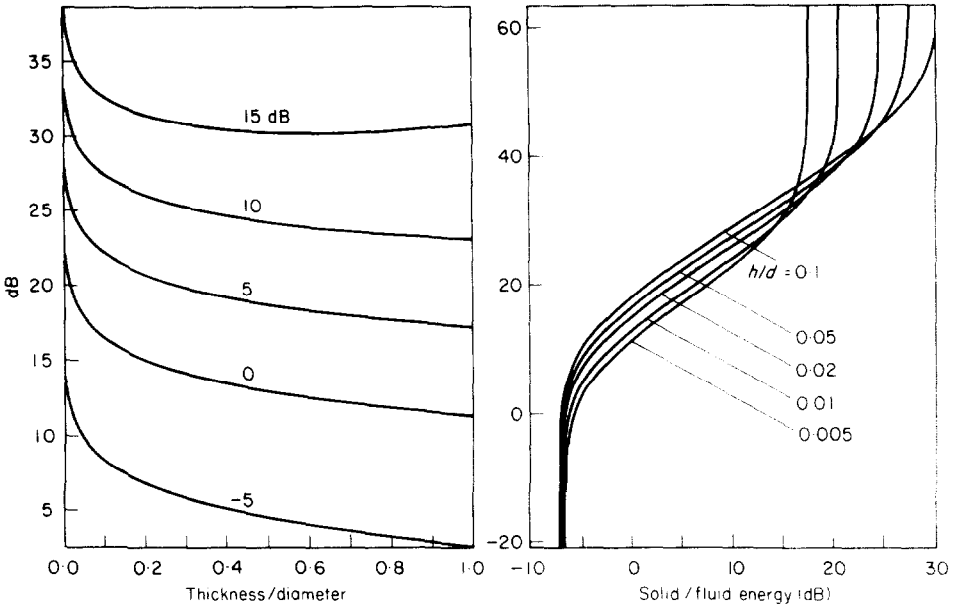

Figure 13. Ratio of amplitudes of l and a waves for rubber pipes filled with water.

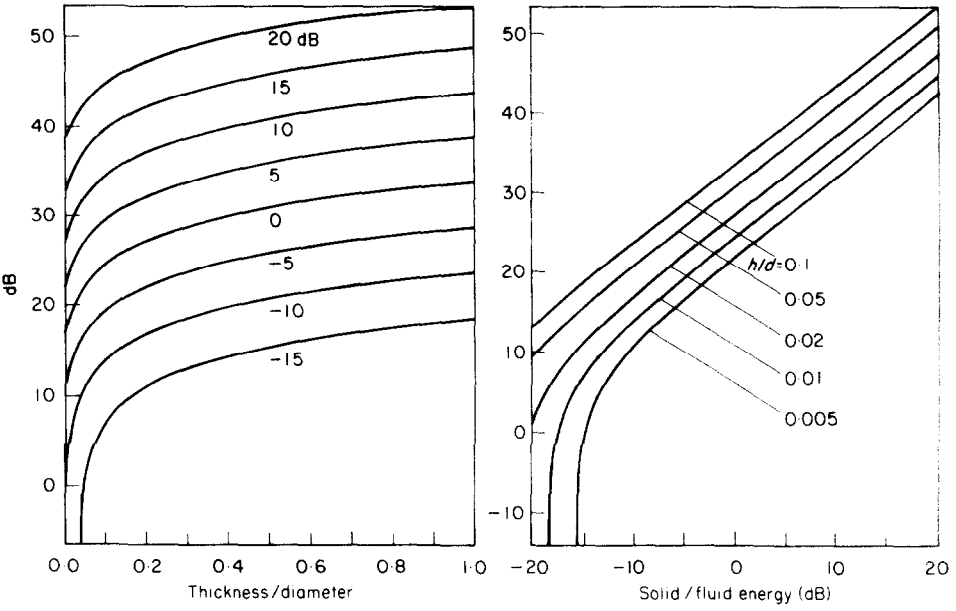

Figure 14. Ratio of amplitudes of l and a waves for rubber pipes containing compressed air (10 bar).

8. CONCLUSIONS

At lower relative frequencies, the dispersion characteristics of each of the four types of travelling wave which can propagate in a fluid-filled pipe can be reasonably reduced to a very simple form (equations (1)). In this way the pipe virtually becomes a rod–beam type waveguide up to the cut-on frequency of the first "lobar" mode, $n=2$. An analysis of the accuracy of simplifications enables determination of the limits of the rod–beam approach.

The expressions (12) and (14) for energy flow in the wall and the fluid, based on the simplified description of vibroacoustical pipe parameters, show that at each particular frequency the flow can be expressed in terms of four differences of squared amplitudes of the four assumed wave types. The amplitudes refer to one out of the three orthogonal components which is dominant for the given wave type (and thus easiest to measure). As already found earlier, the "longitudinal" and the "acoustic" type waves carry energy in both the wall and the fluid, with the solid part mostly due to extensional motions in the axial direction. The bending waves cause very small energy flow in the fluid, while torsional waves do not interfere with the fluid at all.

Since the relationships between all the parameters of pipe and fluid motion are known, energy flow not only in the wall but also in the fluid can in principle be determined from data on the wall surface vibrations only. All that is essentially necessary is to determine the four pairs of wave amplitudes. This means that in practical measurements different wave components have to be "demodulated", or "separated" from the total motion. The procedures described in section 6 and Appendix II enable such a separation to be done by minimizing the number of variables required for measurement. Worked-out examples of the dependence of the vibration amplitudes of the pipe wall on the ratio of energies in the wall and the fluid show that, in practice, separation can be achieved for the usual cases of interest.

When measurement conditions do not satisfy the assumptions made in the analysis, the energy flow in the pipe wall can be obtained by unit-flow detection, according to equations (8), and an additional spatial averaging (equation (10)). As mentioned earlier, in the presence of a fluid in the pipe, some portion of the energy flow fluctuates between the fluid and the solid along the pipe. Thus, measurements by this "direct" method have to be taken at a number of axial positions and the results averaged.

REFERENCES

1. T. C. LIN and G. W. MORGAN 1956 *Journal of the Acoustical Society of America* **28**, 1165–1176. Wave propagation through fluid contained in a cylindrical elastic shell.
2. V. N. MERKULOV, V. YU. PRIKHODKO and V. V. TYUTEKIN 1978 *Akutichesky Zhurnal* **24**, 723–730. Excitation and propagation of normal modes in a thin cylindrical elastic shell filled with fluid (in Russian).
3. C. R. FULLER and F. J. FAHY 1982 *Journal of Sound and Vibration* **81**, 501–518. Characteristics of wave propagation and energy distributions in cylindrical elastic shells filled with fluid.
4. YU. I. BOBROVNITSKY and V. V. TYUTEKIN 1986 *Akusticheskiy Zhurnal* **32**, 598–604. Energy characteristics of composite waveguides (in Russian).
5. J. M. CUSCHIERI 1988 *Journal of the Acoustical Society of America* **83**, 641–646. Excitation and response of piping systems.
6. A. CAUSSE and J. L. TROLLE 1988 *Proceedings of INTER-NOISE* 88, 30 *August–1 September* **1**, 579–582. Dynamic analysis of nuclear plant circuit by vibrational intensity measurement.
7. K. SATO and I. HONDA 1988 *Proceedings of INTER-NOISE* 88, 30 *August–1 September* **1**, 591–594. Application of vibrational power measurement to the piping system in an air conditioner.
8. J. W. VERHEIJ 1982 *Doctoral Thesis, Technische Physische Dienst TNO-TH, Delft, The Netherlands*. Multipath sound transfer from resiliently mounted shipboard machinery.
9. G. PAVIĆ 1986 *Proceedings of XXII International Congress on Acoustics*, 24–31 *July*, D6-6. The influence of curvature on structure-borne acoustical power propagation in a cylindrical circular shell.
10. G. PAVIĆ 1989 *Proceedings of XXIII International Congress on Acoustics*, 24–31 *July* **1**, 193–196. LF acoustical energy flow in axisymmetric motion of fluid-filled pipes.
11. W. FLÜGGE 1973 *Stresses in Shells*. Berlin: Springer-Verlag (second edition).
12. P. M. MORSE and K. U. INGARD 1968 *Theoretical Acoustics*. New York: McGraw-Hill.
13. P. H. WHITE and R. J. SAWLEY 1972 *Transactions of the American Society of Mechanical Engineers Journal of Engineering for Industry* **94**, 746–751. Energy transmission in piping systems and its relation to noise control.

14. P. G. BENTLEY and D. FIRTH 1976 *Computers and Structures* **6**, 187–192. Calculation of basic resonances for acoustic vibration in fast reactors.
15. G. PAVIĆ 1990 *Journal of Sound and Vibration* **142**, 293–310. Vibrational energy flow in elastic circular cylindrical shells.

APPENDIX I: DISPERSION EQUATION FOR A PIPE

The dispersion equation can be written in the form

$$\det [Q] = 0, \tag{A1}$$

where the coefficients of the matrix Q, according to Flügge's model, are

$$Q_{11} = \kappa^2 + [(1-\nu)/2](1+\beta^2)n^2 - \Omega^2, \qquad Q_{12} = Q_{21} = -[(1+\nu)/2]\kappa n,$$
$$Q_{13} = Q_{31} = -\nu\kappa - \beta^2\kappa[\kappa^2 - \{(1-\nu)/2\}n^2], \qquad Q_{22} = n^2 + [(1-\nu)/2](1+\beta^2)\kappa^2 - \Omega^2,$$
$$Q_{23} = Q_{32} = n + [(3-\nu)/2]\beta^2 n\kappa^2, \qquad Q_{33} = 1 - \Omega^2 - Fl + \beta^2[1 - 2n^2 + (\kappa^2 + n^2)^2]. \tag{A2}$$

The non-dimensional term Fl represents external normal loading on the wall. For a shell internally filled with fluid this term is [15]

$$Fl = \Omega^2 \frac{\rho_f}{\rho_s}\frac{a}{h}\left[\sum_{i=0}^{\infty}\frac{(-\xi^2/4)^i}{i!(n+i)!}\right]\left[\sum_{i=0}^{\infty}\frac{(-\xi_2/4)^i(2i+n)}{i!(n+i)!}\right]^{-1}. \tag{A3}$$

Expansion of Fl to first order, applicable for $\kappa \ll 1$, yields

$$n=0: \quad Fl \approx -\frac{\rho_f}{\rho_s}\frac{a}{h}\frac{2}{\psi - \zeta^2}; \qquad n=1: \quad Fl \approx \Omega^2\frac{\rho_f}{\rho_s}\frac{a}{h}. \tag{A4}$$

For $n=0$, the dispersion equation can be expanded in powers of Ω^2, where the terms higher than first can be disregarded when $\Omega \ll 1$. The solution of the equation is then given by

$$\kappa = \zeta\Omega, \tag{A5}$$

where the proportionality coefficient ζ follows from the quadratic equation

$$\zeta^4 - \left(\psi + \frac{2\eta + 1 + \beta^2}{1 - \nu^2 + \beta^2}\right)\zeta^2 + \frac{\psi(1+\beta^2) + 2\eta}{1 - \nu^2 + \beta^2} = 0. \tag{A6}$$

The dispersion equation for $n=1$, after being simplified by neglecting less important terms, results in a formula of Bernoulli–Euler type, equations (1).

The coefficients of the matrix Q determine the ratio between the amplitudes of three displacement components:

$$U/W = (Q_{12}Q_{23} - Q_{13}Q_{22})/(Q_{11}Q_{22} - Q_{12}Q_{21}),$$
$$V/W = (Q_{21}Q_{13} - Q_{11}Q_{23})/(Q_{11}Q_{22} - Q_{12}Q_{21}). \tag{A7}$$

APPENDIX II: EXTRACTION OF AXIAL COMPONENTS OF THE ENERGY FLOW

The quantities to be identified are the differences of the axial displacement squared amplitudes, L and A, as defined in equations (15):

$$L = U_{l+}^2 - U_{l-}^2, \qquad A = U_{a+}^2 - U_{a-}^2.$$

It follows from equations (2) that the axial displacements pertaining to l and a modes, needed for evaluating L and A, can be extracted by using the superposition expressions (17):

$$\mathbf{u}^{+} = \mathrm{j}U_{l+}\boldsymbol{\mu}_{l+} + \mathrm{j}U_{l-}\boldsymbol{\mu}_{l-} + \mathrm{j}U_{a+}\boldsymbol{\mu}_{a+} + \mathrm{j}U_{a-}\boldsymbol{\mu}_{a-}. \tag{A8}$$

Here:

$$\boldsymbol{\mu}_{l\pm} = \exp\{\mp\mathrm{j}\kappa_l(x/a) + \mathrm{j}\varphi_{l\pm}\}, \qquad \boldsymbol{\mu}_{a\pm} = \exp\{\mp\mathrm{j}\kappa_a(x/a) + \mathrm{j}\varphi_{a\pm}\}.$$

Upon introducing the new abbreviations

$$\boldsymbol{\Phi}_l = \mathrm{j}U_{l+}\exp(\mathrm{j}\varphi_{l+}) + \mathrm{j}U_{l-}\exp(\mathrm{j}\varphi_{l-}), \qquad \boldsymbol{\Xi}_l = -(\kappa_l/a)[U_{l+}\exp(\mathrm{j}\varphi_{l+}) - U_{l-}\exp(\mathrm{j}\varphi_{l-})],$$

$$\boldsymbol{\Phi}_a = \mathrm{j}U_{a+}\exp(\mathrm{j}\varphi_{a+}) + \mathrm{j}U_{a-}\exp(\mathrm{j}\varphi_{a-}),$$

$$\boldsymbol{\Xi}_a = -(\kappa_a/a)[U_{a+}\exp(\mathrm{j}\varphi_{a+}) - U_{a-}\exp(\mathrm{j}\varphi_{a-})], \tag{A9}$$

the following relationships emerge from equations (A8), which express the new quantities in terms of the (total) axial displacement u, axial strain $\varepsilon_x = \partial u/\partial x$ and two strain derivatives (all of these are measurable):

$$\boldsymbol{\Phi}_l = -(\kappa_a^2\mathbf{u} + a^2\,\partial\boldsymbol{\varepsilon}_x/\partial x)/(\kappa_l^2 - \kappa_a^2), \qquad \boldsymbol{\Xi}_l = (\kappa_a^2\boldsymbol{\varepsilon}_x + a^2\,\partial^2\boldsymbol{\varepsilon}_x/\partial x^2)/(\kappa_l^2 - \kappa_a^2),$$

$$\boldsymbol{\Phi}_a = -(\kappa_l^2\mathbf{u} + a^2\,\partial\boldsymbol{\varepsilon}_x/\partial x)/(\kappa_a^2 - \kappa_l^2), \qquad \boldsymbol{\Xi}_a = (\kappa_l^2\boldsymbol{\varepsilon}_x + a^2\,\partial^2\boldsymbol{\varepsilon}_x/\partial x^2)/(\kappa_a^2 - \kappa_l^2). \tag{A10}$$

Finally, the time-averaged products of $\boldsymbol{\Phi}$ and corresponding $\boldsymbol{\Xi}$ pairs have to be taken, to produce results directly proportional to the required squared amplitudes differences:

$$\overline{\Xi_l(t)\Phi_l(t)} = (1/2)\,\mathrm{Re}\{\boldsymbol{\Xi}_l\boldsymbol{\Phi}_l^{*}\} = \kappa_l[\omega/(2a)](U_{l+}^2 - U_{l-}^2),$$

$$\overline{\Xi_a(t)\Phi_a(t)} = (1/2)\,\mathrm{Re}\{\boldsymbol{\Xi}_a\boldsymbol{\Phi}_a^{*}\} = \kappa_a[\omega/(2a)](U_{a+}^2 - U_{a-}^2). \tag{A11}$$

APPENDIX III: NOTATION

a	mean radius of the shell
c	velocity of propagation
d	pipe diameter
E	Young's modulus
Fl	fluid loading
h	thickness
H	energy flow
I	intensity
j	imaginary unit
J	Bessel function
k	wavenumber
n	circumferential mode number
p	pressure
P	pressure amplitude
q	displacement (general)
r	radial co-ordinate
t	time
u	axial displacement
U	axial displacement amplitude
v	tangential displacement
V	tangential displacement amplitude
w	radial displacement
W	radial displacement amplitude
x	axial co-ordinate
α	circumferential angle

β $= (h/a)/\sqrt{12}$, relative thickness
γ polarization angle
Γ non-dimensional constant
δ spacing between transducers
ε normal strain
ζ wavenumber constant
η non-dimensional constant
ϑ circumferential angle
κ non-dimensional axial wavenumber
Λ power factor
μ propagation factor
ν Poisson ratio
ξ non-dimensional radial wavenumber
Ξ measurement variable
ρ mass density
φ phase angle
Φ measurement variable
ψ non-dimensional constant
ω angular frequency
Ω non-dimensional frequency

Indices

a acoustic
b bending
f fluid
l longitudinal
s solid
t torsional
$+$ positive direction
$-$ negative direction
0 middle surface

Operators

$\mathbf{C}$ bold letter denotes complex quantity
det determinant
Re real part
$\overline{}$ time average
$\langle\ \rangle$ spatial average
$\cdot$ temporal derivative
$*$ complex conjugate